AIAA JOURNAL
Vol. 36, No. 3, March 1998

Study of Passive Control in a Transonic Shock Wave/Boundary-Layer Interaction

Reynald Bur,* Bernard Corbel,† and Jean Délery‡
ONERA, F-92320 Châtillon, France

Passive control applied to a turbulent shock wave/boundary-layer interaction has been investigated by considering a two-dimensional channel flow. The field has been probed in great detail by using a two-component laser Doppler velocimetry system to execute mean velocity and turbulence measurements. Four different perforated plates have been considered along with the solid wall reference case. These measurements have shown that passive control deeply modifies the inviscid flowfield structure, the single shock being replaced by a lambda shock system. This modified compression induces a substantial reduction of the wave drag associated with the interaction. On the other hand, the combined injection–suction effect taking place in the control region provokes an increase of the viscous drag, which nearly outbalances the reduction in wave drag. It was found that passive control induced a modest decrease of the total drag compared to the solid wall case. Moreover, the experimental wall transpiration velocity distribution in the control region is well represented by the usual laws.

Nomenclature

C_F = total drag coefficient of the surface without and with control
H_i = boundary-layer incompressible shape parameter equal to

$$\frac{\delta_i^*}{\theta_i} = \int_0^\delta \left(1 - \frac{\bar{u}}{\overline{u_e}}\right) dY \Big/ \int_0^\delta \frac{\bar{u}}{\overline{u_e}}\left(1 - \frac{\bar{u}}{\overline{u_e}}\right) dY$$

h = cavity depth
k = turbulent kinetic energy
L = streamwise extent of the control region, 70 mm
M = Mach number
P = porosity of the perforated plate, open area/plate area, %
p = static pressure
p_{st0} = stagnation (reservoir) pressure
T_{st0} = stagnation temperature
U_0 = reference velocity, 377 m/s
u, v = X- and Y-wise instantaneous velocity components
$\bar{u}, \bar{v}$ = mean values of u and v
u', v' = fluctuating parts of u and v
$\overline{u'^2}, \overline{v'^2}$ = turbulent normal stresses
$-\overline{u'v'}$ = turbulent shear stress
X = streamwise coordinate along the channel lower wall, origin at the test section entrance; see Fig. 1
Y = coordinate normal to the channel lower wall
δ = boundary-layer physical thickness
δ^* = boundary-layer displacement thickness equal to

$$\int_0^\delta \left(1 - \frac{\rho\bar{u}}{\rho\overline{u_e}}\right) dY$$

θ = boundary-layer momentum thickness equal to

$$\int_0^\delta \frac{\rho\bar{u}}{\rho_e\overline{u_e}}\left(1 - \frac{\bar{u}}{\overline{u_e}}\right) dY$$

θ^* = boundary-layer mean flow kinetic energy thickness equal to

$$\int_0^\delta \frac{\rho\bar{u}}{\rho_e\overline{u_e}}\left(1 - \frac{\bar{u}^2}{\bar{u}_e^2}\right) dY$$

ρ = density

Subscripts

e = conditions at the local boundary-layer edge
f = conditions at the end of the investigated domain, where X is equal to 365 mm
w = conditions at the channel lower wall in the control region
0 = conditions at the origin of the investigated domain, where X is equal to 220 mm

Presented as Paper 97-0217 at the 35th Aerospace Sciences Meeting, Reno, NV, Jan. 6–9, 1997; received May 6, 1997; revision received Sept. 20, 1997; accepted for publication Oct. 3, 1997.

*Research Scientist, Experimental/Fundamental Aerodynamics Branch.
†Technical Engineer, Experimental/Fundamental Aerodynamics Branch.
‡Head, Experimental/Fundamental Aerodynamics Branch. Member AIAA.

Introduction

SHOCK waves and their interaction with the boundary layer play a major role in determining the performance of transonic transport aircraft. It has been suggested that one way to reduce the harmful effects of strong shock waves at the off-design performance of airfoils is to use a passive control device in the interaction region.

The principle of passive control consists of establishing a natural circulation between the downstream high pressure face of a shock and its upstream low pressure face. This circulation is achieved through a closed cavity, placed underneath the shock foot region, the face in contact with the outer flow being made by a perforated plate. Experimental and theoretical studies have shown that passive control may produce a reduction of airfoil drag, mainly by reducing its wave drag.[1–11] Another advantage of passive control would be to fix the shock location, preventing large amplitude oscillations that may occur at high incidence (buffeting phenomenon). However, the boundary-layer manipulation resulting from the combined injection–suction effect provokes an increase of the viscous drag, which may outbalance the wave drag reduction. Thus, as far as airfoil drag is concerned, the potential benefit of passive control results from a delicate balance between two opposite tendencies.

The objective of this study was to contribute to the understanding and modeling of the physical phenomena involved in a shock wave/boundary-layer interaction under control conditions. The experiments were executed in a transonic channel flow and considered the interaction between the shock crossing the channel and the boundary layer developing on one of the channel walls. This arrangement allowed working with a boundary layer thick enough to permit accurate definition of its properties during the interaction process.

The mean and turbulent properties of the interaction domain were determined mainly by means of laser Doppler velocimetry (LDV) explorations, first, in the absence of control (solid wall reference case) and, second, under passive control conditions for four perforated plates, having different geometrical characteristics. A method to determine the total drag in the control region is proposed to define an optimum passive control configuration. An experimental wall velocity distribution in the control region has been obtained and compared to usual control laws.

Test Setup and Equipment

Test Setup Arrangement

These experiments were executed in the S8 transonic–supersonic wind tunnel of the ONERA Fluid Mechanics Laboratory at Chalais-Meudon, France. This facility is a continuous wind tunnel supplied with desiccated atmospheric air. The stagnation conditions are $p_{st0} = 92{,}000 \pm 50$ Pa and $T_{st0} = 300 \pm 3$ K. The test setup, shown in Fig. 1, consists of a transonic channel having a test section with a height of 100 mm and a span of 120 mm. The lower wall is rectilinear, whereas the upper wall is a contoured profile designed to produce a uniform supersonic flow of nominal Mach number equal to 1.4.

A second throat, of adjustable cross section, is placed in the test section outlet to produce by choking effect a shock wave whose position can be adjusted in a continuous and precise manner. It also isolates the flowfield from pressure perturbations emanating from downstream ducts, reducing unwanted shock oscillations.

Passive control is applied on the rectilinear lower wall in a region where the outer inviscid flow Mach number is $M_0 = 1.34$. The length L of the control cavity has been defined in such a way as to approximately reproduce the ratio L/δ_0 existing on an airfoil, i.e., $L/\delta_0 \simeq 18$. In the present experiments $\delta_0 \simeq 4$ mm; therefore, the value $L = 70$ mm has been adopted for all test cases (Fig. 1). Its depth h is equal to 60 mm. A first study[12] has demonstrated that h has a negligible influence on the control mechanism, provided it is not too small (at least 10 mm for the present conditions). The interchangeable perforated plate is fixed to the wall, upstream and downstream of the cavity, with the plate made flush with the wall. For the study of the interaction without passive control (reference case), a rectilinear solid wall extending from the entrance to the end of the channel was manufactured to avoid the perturbations caused by junctions between different parts.

The pressure orifices were located in the vertical median plane of the test setup, with seven of them installed on the plates to determine the pressure distribution in the control region. Moreover, five pressure taps were located on the bottom part of the cavity.

Techniques of Investigation

The flows under study were qualified by schlieren visualizations and quantified by measurements of wall pressure distributions and (instantaneous) velocity distributions.

For the present nominally two-dimensional flow, the latter were obtained with a two-component LDV system.[13] The light source is a 5-W argon laser beam, which is separated into two beams of wavelength 0.488 μm (blue) and 0.5145 μm (green). These beams are split by classical beam splitters and traverse Bragg cells to enable the system to detect the velocity direction. The four beams are focused to constitute two fringe patterns inside the measuring volume, whose diameter was equal to 0.2 mm. The blue and green fringe spacings are 13.30 and 13.82 μm, respectively. The LDV system was operated in the forward scattering mode. The flow is seeded with submicronic (0.5-μm-diam) droplets of parafine oil injected in the wind tunnel settling chamber.

The flowfields have been explored along 30 vertical lines (Y direction), extending from the surface ($Y = 0$) to an altitude $Y = 22$ mm and contained in the test section median plane. Their streamwise locations X were in the range $220 \leq X(\text{mm}) \leq 365$ (including the control region). Reliable measurements with the LDV system, in the two-component version, were limited to a minimum distance of 0.3 mm from the wall.

At each measurement point, a sample of couples of the instantaneous values of the velocity components u and v is acquired for further processing. The size of the sample, equal to 2000, gives an acceptable statistical uncertainty for the first- and second-order statistical moments. The determination of the mean velocity components allows the local Mach number to be computed and the boundary-layer global properties (δ^*, θ, θ^*, and H_i) to be defined. The density and sound velocity are computed by assuming constant stagnation temperature throughout the flow. The two-component version of the LDV system did not allow the determination of the spanwise velocity component w. Thus, the turbulent kinetic energy k has been estimated by the following formula:

$$k = \tfrac{1}{2}\left[\overline{u'^2} + \overline{v'^2} + \tfrac{1}{2}\left(\overline{u'^2} + \overline{v'^2}\right)\right]$$

The LDV components give the field quantities with an accuracy depending on uncertainties affecting the LDV system calibration (uncertainties on the fringe distance, on the Bragg frequency), the determination by the counters of the frequency of the light scattered by the particles, and the statistical treatment of the sample.

For these experiments, the field properties have been determined with a precision of 1) 1% of the maximum velocity modulus for the mean velocity components, 2) less than or equal to 8% concerning the normal stress components of the Reynolds tensor, and 3) less than or equal to 10% concerning the turbulent shear stress component.

Tested Configurations

In addition to the solid wall reference case, four different plates, numbered 1–4, whose nominal characteristics are given in Table 1, have been tested. The holes were drilled by an electron beam technique. The thickness of the plates was equal to 1 mm. All of the plates have the same porosity, i.e., $P = 5.67\%$. For plates 1 and 2, the holes are everywhere normal to the surface. For plates 3 and 4, the holes are inclined with respect to the surface (in the downstream direction) in the upstream half of the plate and normal to it in its downstream half.

Table 1 Nominal characteristics of the tested plates

Plate number	Porosity, %	Hole diameter, mm	Hole inclination, deg
1	5.67	0.15	90
2	5.67	0.30	90
3	5.67	0.15	45 and 90
4	5.67	0.30	45 and 90

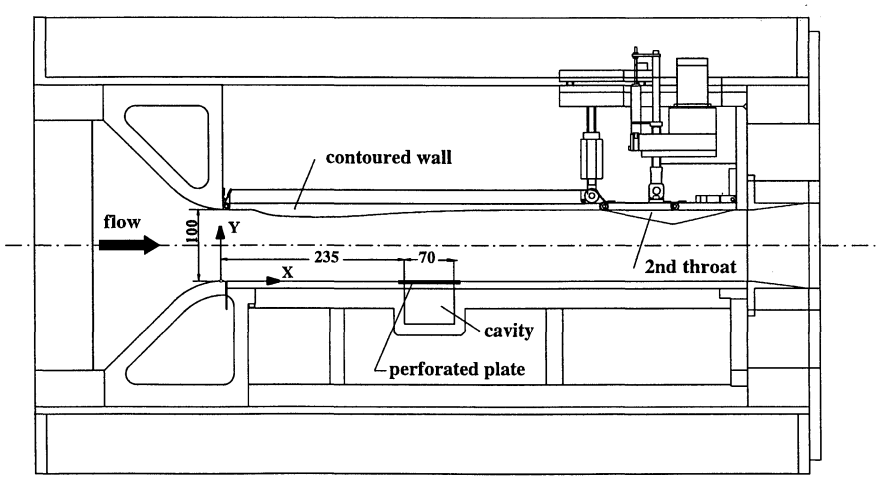

Fig. 1 Passive control experimental setup in the S8 wind tunnel. Dimensions are in millimeters.

The location of the shock wave in the outer part of the flow, i.e., outside the interaction region, was fixed at middistance between the origin and the end of the control region.

Results and Discussion

Flow Visualizations

The schlieren photograph in Fig. 2 shows the flow structure for the reference case. One notes the thickening of the boundary layer in the shock foot region and the associated compression wave pattern forming in the outer inviscid flow. This front zone is followed by a small triangular region of still supersonic flow terminated by a nearly normal shock, sometimes called the trailing shock. The compression waves and the trailing shock meet in a region from which the single shock crossing the channel starts. The present flow pattern corresponds to a situation nearly coincident with incipient shock-induced separation, which occurs for an upstream Mach number of 1.30. The present value $M_0 = 1.34$ should lead to the formation of a tiny separation bubble. However, LDV measurements have not detected negative values for the streamwise velocity component. Thus, if it exists, the bubble must be excessively small.

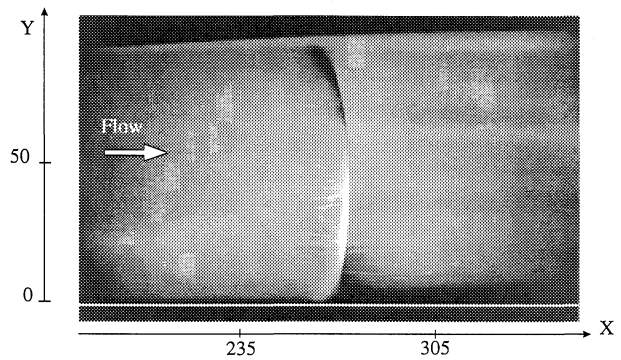

Fig. 2 Schlieren photograph of the flowfield, reference case (solid wall).

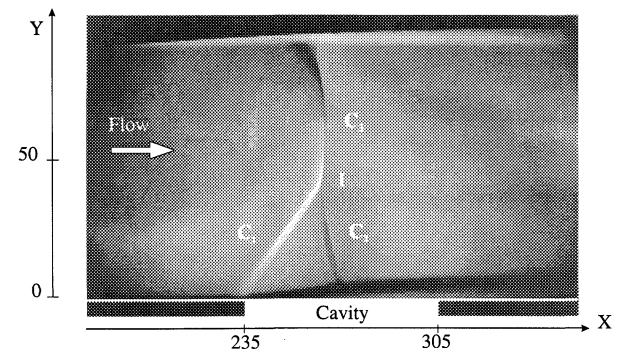

Fig. 3 Schlieren photograph of the flowfield, with passive control (plate 2).

The schlieren visualization of the flow under passive control (with plate 2) is shown in Fig. 3. Now, the boundary layer starts to thicken suddenly at the cavity origin. Then, it takes a wedge-like shape until it meets with the trailing shock; afterward, its thickness remains nearly constant. Hence, passive control can induce an increase of the viscous drag. The rapid thickening of the boundary layer, which is provoked by the injection effect taking place in the upstream part of the control region, is felt by the contiguous supersonic flow as a ramp effect. This leads to the formation of the oblique leading shock C_1, downstream of which the Mach number is still supersonic. This supersonic region is terminated by the trailing shock C_2, through which the velocity vector changes from an upward direction to become nearly parallel to the wall. The two shocks C_1 and C_2 meet at the triple point I, from which starts the single shock C_3, to constitute a well-defined lambda shape. In this case, a single strong shock is replaced by two weaker shocks over a large part of the channel flow. The rise in entropy (or loss in stagnation pressure) is smaller through the consecutive shocks C_1 and C_2 than across the single shock C_3. Therefore, passive control can reduce the wave drag.

The schlieren pictures obtained with plates 1, 3, and 4 have shown similar modifications of the flow structure in the control region.

Surface Pressure Distributions

The surface pressure distributions on the channel lower wall for the reference case and the four control cases are plotted in Fig. 4.

The decreasing part of the distribution corresponds to the expansion in the supersonic part of the channel. In the reference case, the interaction with the shock wave produces a rapid rise of the pressure to a downstream nearly constant level $p/p_{st0} = 0.63$, giving an outer flow Mach number equal to 0.84. The general shape of the curve is typical of a transonic interaction without (noticeable) separation.

The surface pressure distribution obtained with plate 2 shows that the start of the pressure rise practically coincides with the cavity forward edge. The local outer flow Mach number just upstream of this abscissa is equal to 1.31. The curve exhibits the three inflection points typical of interaction with separation. In this situation, the pressure first undergoes a rapid rise associated with the leading shock C_1. Then, the slope decreases with the tendency (weakly marked in the present case) toward an intermediate constant level. Thereafter, the pressure gradient increases again, remaining less intense than in the first part of the interaction. Finally, the pressure tends toward the constant downstream level.

The surface pressure distributions measured for the three other plates lead to no obvious differences between the four distributions. It is to be noticed that the cavity pressure is slightly higher for

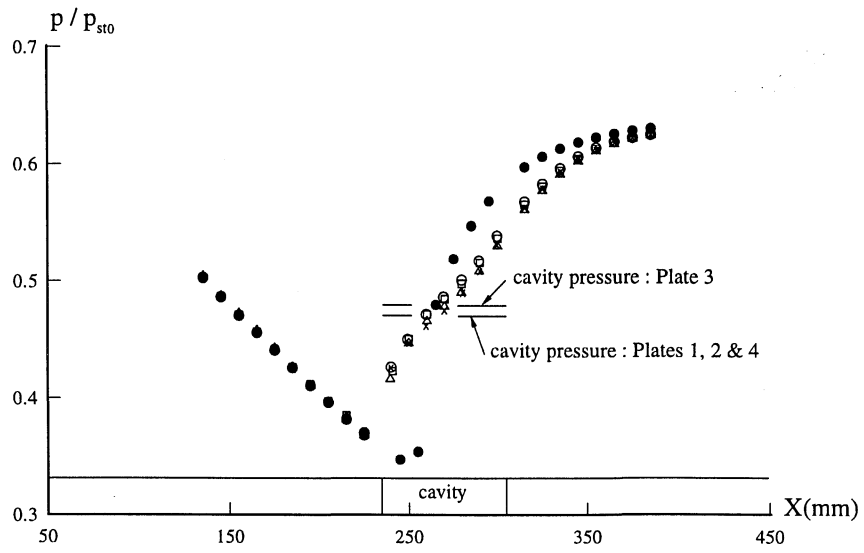

Fig. 4 Comparison of the surface pressure distributions: ●, reference case; ○, plate 1; ×, plate 2; □, plate 3; and △, plate 4.

plate 3 than for the other plates ($p/p_{st0} = 0.480$ instead of 0.472). No convincing explanation of this difference has been found. Hence, by considering these results as well as the visualizations, it is not possible to define a significant influence of the diameter and/or inclination of the plate holes.

LDV Measurements

Because the influence of the plate characteristics is weak, only the case of plate 2 will be thoroughly discussed and compared with the reference case.

The contour lines of the Mach number are traced in Figs. 5 and 6, for the reference case and the passive control case respectively, adopting the same scale (Figs. 5a and 6a) for the X- and Y-wise distances and with an Y-wise dilatation (Figs. 5b and 6b) to have a better resolution of the boundary-layer region. The apparent thickness of the shock is due to an insufficient refinement of the measurement mesh (X-wise spacing of 5 mm). Figure 6 shows that the leading shock C_1 provokes a first supersonic compression of the flow from an upstream Mach number of 1.30 to a downstream value of 1.18. In the region situated between C_1 and C_2, the Mach number varies from 1.18 to 1.10 as the flow undergoes an isentropic compression. A region of supersonic flow, bounded by iso-Mach line $M = 1$, exists downstream of C_2 as the outer inviscid flow undergoes a nearly isentropic compression to a Mach number of 0.86 at the end of the explored region.

The longitudinal evolutions of the boundary-layer characteristic thicknesses are plotted in Fig. 7. For the flow under control, the displacement thickness δ^* reaches a maximum near of 4.8 mm at $X \simeq 315$ mm, leading to a ratio $\delta^*_{max}/\delta^*_0 = 9.32$, to be compared with the value 5.10 of the reference case. Whereas the thickening of the boundary layer is comparable in the two cases, this large difference in the increase of δ^* proves that passive control provokes a greater destabilization of the boundary layer; i.e., the velocity profiles are less full. After going through its maximum, δ^* decreases slowly in both cases. The evolution of the momentum thickness θ is of special interest because it is a measure of momentum loss

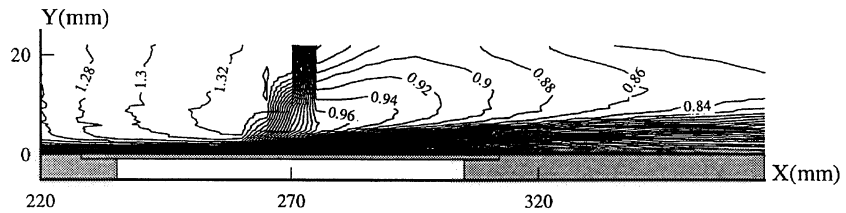

a) Identical longitudinal and normal scales

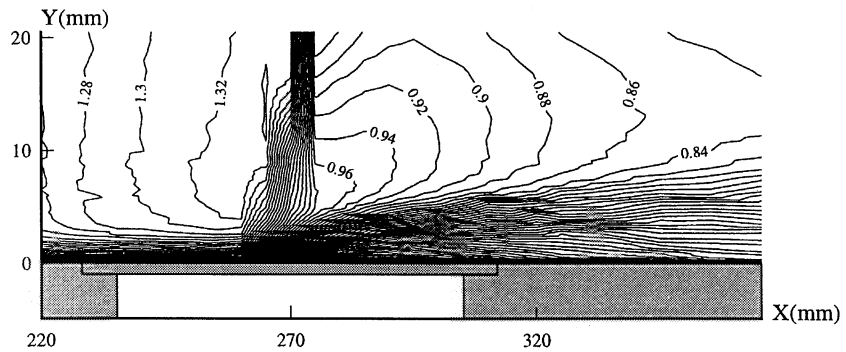

b) Enlarged normal scale

Fig. 5 Contour lines of the Mach number, reference case (solid wall).

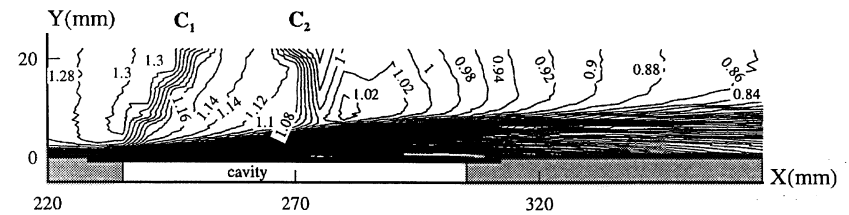

a) Identical longitudinal and normal scales

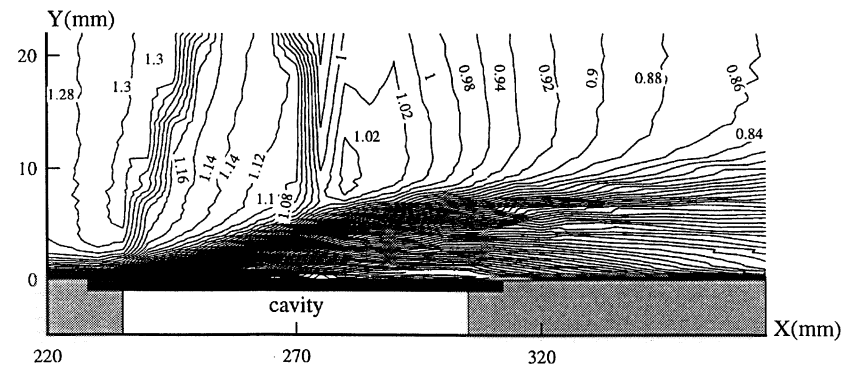

b) Enlarged normal scale

Fig. 6 Contour lines of the Mach number, with passive control (plate 2).

Table 2 Typical values of the boundary-layer global characteristics

	Solid wall	Plate 1	Plate 2	Plate 3	Plate 4
$\delta^*_{max}/\delta^*_0$	5.10	9.06	9.32	9.33	9.38
θ_f/θ_0	6.14	9.27	9.32	9.32	8.98
$H_{i\,max}$	2.50	3.50	3.57	3.65	3.70

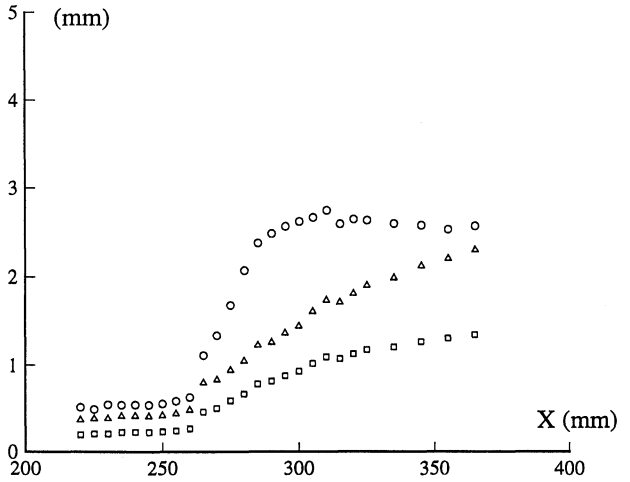

Reference case (solid wall)

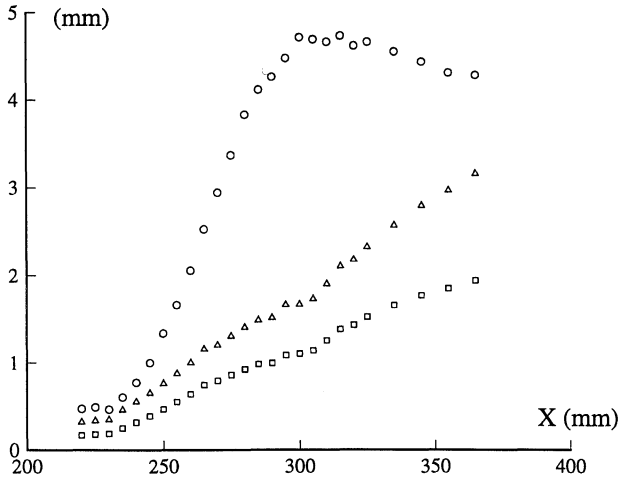

With passive control (plate 2)

Fig. 7 Evolutions of the boundary-layer characteristic thicknesses: ○, δ^*; □, θ; and △, θ^*.

undergone by the flow because of dissipative effects. For the flow under control, θ reaches a maximum near of 2 mm at the end of the explorated domain, to which a ratio $\theta_f/\theta_0 = 9.32$ corresponds, to be compared with the value 6.14 of the reference case. It can, therefore, be expected that the viscous drag is greater when passive control is applied.

The results relative to the other tested plates lead to no obvious effect of the plate characteristics on the mean flow properties. Table 2 summarizes typical values of the boundary-layer global characteristics for all of the tested configurations by giving the final value of θ and the maximum values reached by δ^* and H_i. These results do not show any significant effect of the hole diameter or inclination of the plates, the scatter being mainly due to measurement uncertainty.

The turbulent field properties are strongly modified by the presence of passive control in the interaction region. To allow a comparison between the reference case and all of the tested plates, the Xwise variations of the local maxima of the turbulent kinetic energy k and shear stress $-\overline{u'v'}$ are plotted in Fig. 8. Passive control produces a higher rise in turbulence levels, which is mainly due to the larger distortion of the velocity profiles. The plots reveal a somewhat different behavior between plates with normal holes (plates 1 and 2) and inclined holes (plates 3 and 4), the rise in turbulent kinetic energy being more important for the inclined holes. The effect on the shear stress is less significant. The plots also exhibit the out phasing between k and $-\overline{u'v'}$, the maxima in $-\overline{u'v'}$ occurring farther downstream than the one in k for each configuration. This lag of the shear stress is a feature commonly observed in shock wave/boundary-layer interactions.[14]

Total Drag Coefficient in the Control Region

One way to evaluate the efficiency of the passive control device is to compute the total drag force F (and its associated coefficient C_F) acting on the surface where control is applied, for each tested plate and the solid wall. For this calculation, the measured flow properties were used. The drag computed here is the component of the force applied to an element of surface (chosen as a portion of the channel lower surface). This force is determined by calculating the momentum balance for the control volume S defined as follows.

1) The surface element located at ordinate $Y = 0$ comprises the region between the abscissas $X = 220$ and 365 mm (the first and last stations of the LDV probing, respectively) and includes the region of control.

2) The upper boundary is rectilinear, parallel to the surface, and placed at an ordinate higher than the maximum boundary-layer thickness.

3) The entry and exit sections are perpendicular to the surface and located at the abscissas $X = 220$ and 365 mm, respectively.

The momentum balance gives on this control surface S:

$$\iint_S [\boldsymbol{P} + \boldsymbol{F} + \rho(\boldsymbol{V}\cdot\boldsymbol{n})\boldsymbol{V}]\,\mathrm{d}S = \boldsymbol{0}$$

where the $\boldsymbol{P}$ and $\boldsymbol{F}$ vectors are associated with pressure and viscous forces, respectively; $\boldsymbol{V}$ is the velocity vector; and $\boldsymbol{n}$ the unit normal vector relative to the considered element of surface.

The projection of this relation on the longitudinal X axis allows obtaining the friction drag F. To evaluate this balance, it is assumed that the pressure in the entry and exit sections is constant along Y, which may constitute an approximation. Also, having seen that the pressure in the cavity is practically constant and that the velocities are quite below those of the external flow, the possibility of the cavity contribution to the drag was not considered. The associated total drag coefficient is defined as

$$C_F = \frac{F}{\frac{1}{2}\rho_0 U_0^2}$$

where F is the friction force per unit of surface and the reference values ρ_0 and U_0 are the freestream values.

Table 3 gives the values of C_F and indicates the percentage of decrease in C_F by comparison with the solid wall, defined as

$$\Delta C_F = \frac{C_{F(\text{solid})} - C_{F(\text{porous})}}{C_{F(\text{solid})}}$$

These results show a slight decrease (around 4%) of the perforated plates average coefficient value compared to the solid wall value. This reduction of drag must be taken with caution because of measurement uncertainties, especially on the mean velocity components. Moreover, the results do not give clear indications about differences that could be due to the characteristics of the plates (diameter and inclination of the holes).

Transpiration Velocity Distributions

The present measurements result in a distribution of the nonzero (transpiration) velocity component v_w normal to the surface where control is applied. The scatter of these measurements has several origins: first, there is the limited accuracy of the LDV measurements (the uncertainty in v is of the order of 1% of the outer flow velocity, i.e., about 3 m/s); second, v_w is not uniformly distributed, injection or suction being performed through discrete holes (the measuring

Table 3 Total drag coefficient of the surface without and with passive control

	Solid wall	Plate 1	Plate 2	Plate 3	Plate 4
C_F	0.00991	0.00972	0.00926	0.00946	0.00952
ΔC_F,%	——	1.9	6.6	4.5	3.9

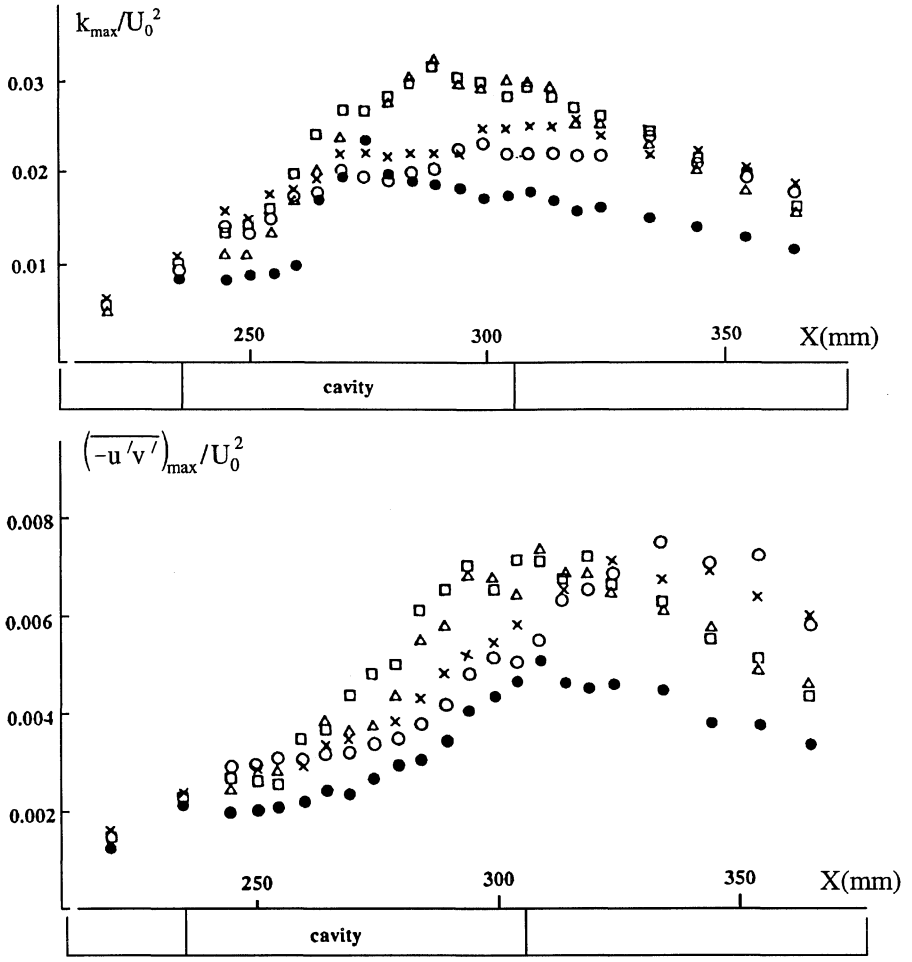

Fig. 8 Streamwise variations of the turbulent kinetic energy and shear stress maxima: ●, reference case; ○, plate 1; ×, plate 2; □, plate 3; and △, plate 4.

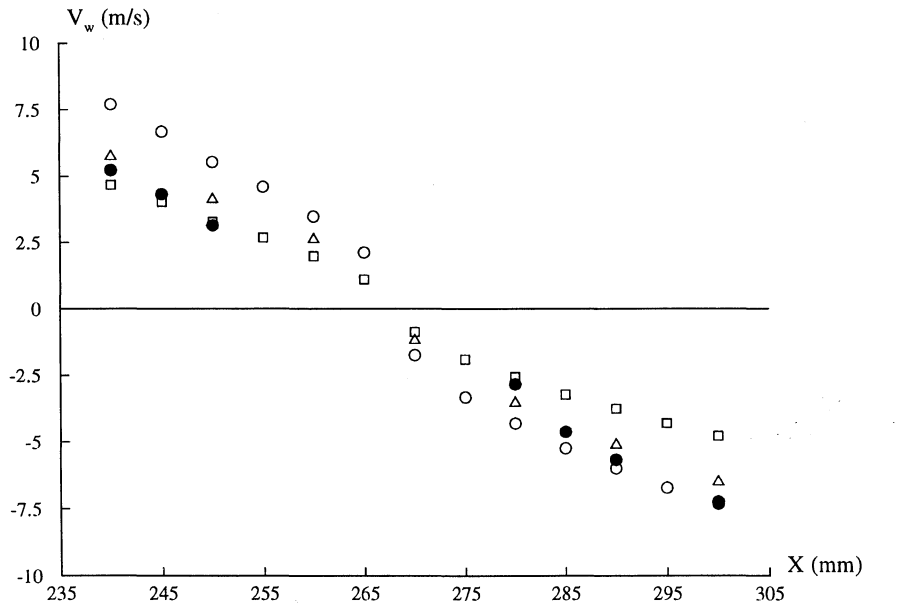

Fig. 9 Transpiration velocity distributions for plate 2; comparison of semiempirical and averaged experimental laws: □, Poll[16] law; ○, isentropic law[15]; △, Bohning and Doerffer[9] law; and ●, experimental distribution.

volume has to be aligned with the holes of the plate); and third, slight deformations of the perforated plate due to the pressure difference occur, rendering the exact location of the measurement point relatively to the wall difficult. Moreover, at the retained altitude (0.3 mm from the plate), the experimental normal velocity v_w distribution is an approximation of the one existing at the surface of the perforated plate.

One can extrapolate from these LDV measurements an experimental law with higher (and more accurate) velocities, respectively, at the beginning and the end of the plate. This experimental law is compared to semiempirical control laws used as wall boundary conditions in numerical approaches to model the injection–suction effect in the control region. The retained control laws are the isentropic law of Abrahamson and Brower,[15] the calibration law of Poll et al.,[16] and a law proposed by Bohning and Doerffer.[9] These semiempirical laws give the transpiration velocities by using the measured surface pressure distribution along the control region. In Fig. 9, a comparison between different transpiration velocity

distributions is shown for plate 2. All of the curves fit rather well with the experimental distribution, the law of Bohning and Doerffer being the best in predicting both the injection and suction velocities. Because of the large uncertainty of the near zero velocity measurements, the behavior of the control laws in this region cannot be discussed.

Conclusions

A detailed experimental investigation of transonic shock wave/boundary-layer interaction under passive control conditions has been performed in a channel type flow. The solid wall reference case and four passive control configurations, with different perforated plates, have been studied by using a two-component LDV system to determine the mean and turbulent flowfield properties.

Passive control induces a clear reduction of the wave drag, the compression being achieved through a two-shock system instead of a single strong shock, while the viscous drag of the boundary layer is significantly increased. In the present situation, the balance tends to be slightly positive but the gain is too small to deduce clear tendencies about the effect of the characteristics of the tested perforated plates (diameter and inclination of the holes) and also to propose an optimal passive control device.

Considering the modest gain achieved with passive control, future studies will be oriented toward the consideration of active control where suction is performed in the cavity. Also, a combination of passive and active control can be foreseen to limit boundary-layer thickening, while maintaining the reduction in wave drag achieved through passive control.

In addition, the present experiments provide well-documented test cases to validate or/and improve the Navier–Stokes codes.

Acknowledgments

The present research was accomplished with the financial support of the European Union through the EUROSHOCK I project. The perforated plates were provided by DASA–Airbus. The laser Doppler velocimetry measurements were performed by the Laser Measurement Group of the Aerodynamics Department of ONERA.

References

[1]Thiede, P., and Krogmann, P., "Passive Control of Transonic Shock/Boundary Layer Interaction," *IUTAM Symposium Transsonicum III* (Göttingen, Germany), Springer–Verlag, Berlin, 1989.

[2]Bohning, R., and Jungbluth, H., "Turbulent Shock/Boundary Layer Interaction with Control. Theory and Experiment," *IUTAM Symposium Transsonicum III* (Göttingen, Germany), Springer–Verlag, Berlin, 1989.

[3]Raghunathan, S., and McIlwain, S. T., "Further Investigations of Transonic Shock Wave/Boundary-Layer Interaction with Passive Control," *Journal of Aircraft*, Vol. 27, No. 1, 1990, pp. 60–65.

[4]Kim, I., and Chokani, N., "Navier–Stokes Study of Supersonic Cavity Flowfield with Passive Control," *Journal of Aircraft*, Vol. 29, No. 2, 1992, pp. 217–223.

[5]Bur, R., "Passive Control of a Shock Wave/Turbulent Boundary Layer Interaction in a Transonic Flow," *La Recherche Aérospatiale*, No. 1992-6, 1992, pp. 11–30.

[6]Chokani, N., and Squire, L. C., "Transonic Shock Wave/Turbulent Boundary Layer Interactions on a Porous Surface," *Aeronautical Journal*, Vol. 97, May 1993, pp. 163–170.

[7]Schnerr, G. H., Dohrmann, U., Sadi, O., and Zierep, J., "Numerical and Experimental Investigation of Passive Control of the Shock/Boundary Layer Interaction in a Transonic Compressor Cascade," ICFM-II, Beijing, PRC, July 1993.

[8]Kim, I., and Sung, B., "Computation of Passively Controlled Transonic Wing," *Journal of Aircraft*, Vol. 32, No. 2, 1995, pp. 349–354.

[9]Bohning, R., and Doerffer, P., "Wind Tunnel Tests of Shock/Boundary Layer Interaction with Passive Control. Porous Wall Flow Investigation. Numerical Simulation of the Wind Tunnel Tests," EUROSHOCK TR AER 2-92-49/1.3, Karlsruhe Univ., Karlsruhe, Germany, Dec. 1995.

[10]Yeung, A. F. K., Squire, L. C., and Faucher, X., "The Passive Control of the Interaction between Swept Shocks and Boundary Layers," EUROSHOCK TR AER 2-92-49/1.2, Cambridge Univ., Cambridge, England, UK, 1995.

[11]Bur, R., and Délery, J., "Study of Passive Control Applied to a Transonic Shock Wave/Boundary Layer Interaction," EUROSHOCK TR AER 2-92-49/1.4, ONERA, Châtillon, France, Jan. 1996.

[12]Chanetz, B., and Pot, T., "Etude fondamentale sur le contrôle passif appliqué à une interaction onde de choc/couche limite en transsonique. Premiers résultats d'essais," ONERA, RT 75/7078 AN, Châtillon, France, July 1988.

[13]Boutier, A., d'Humières, C., and Soulevant, D., "Three Dimensional Laser Velocimetry: A Review," *2nd International Symposium on Applications of Laser Anemometry to Fluid Mechanics* (Lisbon, Portugal), 1984.

[14]Délery, J., "Experimental Investigation of Turbulence Properties in Transonic Shock/Boundary Layer Interactions," *AIAA Journal*, Vol. 21, No. 2, 1983, pp. 180–185.

[15]Abrahamson, K. W., and Brower, D. L., "An Empirical Boundary Condition for Numerical Simulation of Porous Plate Bleed Flows," AIAA Paper 88-0306, Jan. 1988.

[16]Poll, D. I. A., Danks, M., and Humphreys, B. E., "The Aerodynamic Performance of Laser Drilled Sheets," *Proceedings of the First European Forum on Laminar Flow Technology* (Hamburg, Germany), 1992, pp. 274–277.

P. R. Bandyopadhyay
Associate Editor